Chemical Engineering Journal 330 (2017) 531–540

Contents lists available at ScienceDirect

Chemical Engineering Journal

journal homepage: www.elsevier.com/locate/cej

Concurrent photocatalytic and filtration processes using doped TiO_2 coated quartz fiber membranes in a photocatalytic membrane reactor

Mélisa Hatat-Fraile[a,1], Robert Liang[a,b,*,1], Maricor J. Arlos[c], Rui Xiu He[a,b], Peng Peng[d,e], Mark R. Servos[c], Y. Norman Zhou[a,b]

[a] Department of Mechanical and Mechatronics Engineering, University of Waterloo, 200 University Avenue West, Waterloo, ON N2L 3G1, Canada
[b] Waterloo Institute for Nanotechnology, University of Waterloo, 200 University Avenue West, Waterloo, ON N2L 3G1, Canada
[c] Department of Biology, University of Waterloo, 200 University Avenue West, Waterloo, ON N2L 3G1, Canada
[d] School of Mechanical Engineering and Automation, Beihang University, 37 Xueyuan Rd, Beijing 100191, China
[e] International Research Institute for Multidisciplinary Science, Beihang University, 37 Xueyuan Rd, Beijing 100191, China

ARTICLE INFO

Keywords:
Photocatalysis
Membrane filtration
Doping
Titanium dioxide
Surface adsorption

ABSTRACT

Titanium dioxide (TiO_2) composite fiber membranes were prepared by means of sol-gel dip coating methods and were subsequently tested in a photocatalytic membrane reactor (PMR) experiment that incorporated two pollutant removal processes: dead-end filtration and photocatalytic degradation. TiO_2 nanoparticle suspensions were initially prepared using the sol-gel synthesis. Quartz fiber filters were immediately dip coated with undoped and doped TiO_2 sols producing three types of membranes: undoped, nitrogen-doped, and boron-doped TiO_2. The synthesized composite filters were analyzed for their (i) morphology using scanning electron microscopy and (ii) crystal structure using Raman spectroscopy and X-ray diffraction. Chemical composition and chemical bonding of the membranes were determined using X-ray photoelectron spectroscopy. The permeability performance of the membranes was analyzed by measuring the flux using deionized water and the removal of a representative organic pollutant, acid orange 7 (dye), was measured. The experiments were conducted in the PMR under dark and ultraviolet illumination. The removal of dye was improved when undoped and doped TiO_2 filters were used in place of a bare quartz fiber filter, except in the case when boron was used at a low doping concentration. The study demonstrates that optimization of doping parameters, such as the type of dopant (nitrogen or boron) and concentration, on TiO_2 filters can improve the removal rates of model molecule using ultraviolet A irradiation.

1. Introduction

Water pollution caused by refractory organic compounds – pharmaceuticals, pesticides, and organic dyes – is a prevalent problem. These compounds are difficult to remove using conventional water treatment methods, such as adsorption, flocculation, and biological treatments [1,2]. Membrane filtration and advanced oxidation processes (AOPs) can remove these compounds effectively, but have drawbacks regarding secondary costs associated with their implementation. Membrane filtration can be used to remove organic compounds, particulates, and microorganisms [3,4], but these same pollutants can limit the lifetime of the membrane via fouling. Fouling limits the operation due to a reduction of filtration performance from the accumulation of particles on the surface. Chemical disinfection can be used to mitigate fouling, but it requires high dosages to be effective and can be costly [5].

For several decades, AOPs have been used to remove refractory organic pollutants through the generation of highly oxidative radical species, including hydroxyl ($HO^{\cdot}$), superoxide ($O_2^{\cdot-}$), and perhydroxyl ($HOO^{\cdot}$) radicals [6]. These radicals oxidize organic compounds and may lead to their mineralization into CO_2, H_2O, or mineral acids, provided sufficient exposure and reaction time [7,8]. Semiconductor photocatalysis, a passive AOP, uses a photocatalyst, often titanium dioxide (TiO_2), in conjunction with a light source to excite electrons from the valence band to the conduction band. The main advantage of semiconductor photocatalysis is the generation of a renewable oxidant source compared to other AOPs which employ a consumable oxidant source, such as hydrogen peroxide (H_2O_2) with UV, or ozonation. TiO_2 is often used as a photocatalyst due to its chemical and thermal stability, non-toxicity, and lower cost compared to other photocatalysts. It is

* Corresponding author at: Department of Mechanical and Mechatronics Engineering, University of Waterloo, 200 University Avenue West, Waterloo, ON N2L 3G1, Canada.
E-mail addresses: rliang@uwaterloo.ca, rliang66@gmail.com (R. Liang).
[1] Equal contribution to authorship.

http://dx.doi.org/10.1016/j.cej.2017.07.141
Received 13 April 2017; Received in revised form 11 July 2017; Accepted 23 July 2017
Available online 24 July 2017
1385-8947/

often used in slurry batch setups, which offer high organic degradation rates [9–11]. However, the major drawback of heterogenous photocatalysis in slurry reactors is the introduction of an additional step and associated costs to remove the catalyst particulates from the liquid phase to prevent secondary contamination of treated water effluents. Current methods of separation, such as gravity settling and centrifugation, are neither feasible nor cost-effective due to the low density and nano-scale size of TiO_2 [12]. Immobilized TiO_2 nanoparticles on a substrate offers a potential solution and has been explored previously [13–18]. Some of the types of substrates that have been used to immobilize TiO_2 include glass [19], metals [20], activated carbon [21], polymers [22–26], inorganic membranes [27], alumina [28], and silica paper [29].

TiO_2 thin films can be adhered onto a substrate using reactive Ti precursors, or sol-gels, which allow for chemical bonding with various substrates [15,19,30]. A catalyst film is formed at the induction period of the sol-gel process and the reaction takes place in an alcoholic solution containing TiO_2 alkoxide ($Ti(OR)_4$) and water as precursors. The chemistry of the process is a combination of hydrolysis and condensation reactions [31,32], which are as follows:

$$Ti(OR)_4 + H_2O \rightarrow Ti(OR)_3OH + ROH \quad (1)$$

$$(RO)_3Ti{-}OH + OH{-}Ti(OR)_3 \rightarrow (RO)_3Ti{-}O{-}Ti(OR)_3 + H_2O \quad (2)$$

$$(RO)_3Ti{-}OH + RO{-}Ti(OR)_3 \rightarrow (RO)_3Ti{-}O{-}Ti(OR)_3 + R{-}OH. \quad (3)$$

The study focuses on using UV irradiation at $\lambda = 365$ nm, rather than solar simulated light, using undoped and doped TiO_2 coatings on filters because the most commonly used light sources are artificial UV lamps that allow for higher photon fluxes and consistent light output [33]. Doping TiO_2 decreases the bandgap and is achieved by modifying TiO_2 with metals [34], non-metals [35–37], or coupling TiO_2 with other narrow bandgap semiconductors. Choi et al. studied the photoactivity of metal doped TiO_2 using 21 different dopants, including ruthenium (Ru), molybdenum (Mo), osmium (Os), rhenium (Re), vanadium (V), and rhodium (Rh) [38]. Other metal dopants have been investigated as well, such as copper (Cu) [39], zinc (Zn) [40], iron (Fe) [41].

Doping with non-metal atoms, such as nitrogen (N) [42–47], boron (B) [48], and sulfur (S) [49], has been shown to increase the photocatalytic removal efficiency of organic compounds using TiO_2 photocatalysts under visible light irradiation, and also change the morphology of the photocatalysts [50]. However, their effectiveness under UVA light irradiation only (λ = 320–400 nm), a common UV source, against undoped TiO_2 has not been evaluated extensively.

The present study is focused on combining filtration and photocatalytic processes in a dead-end PMR setup using immobilized undoped TiO_2, N-TiO_2, and B-TiO_2 onto quartz fiber filters (QFF). Undoped and doped TiO_2 QFF was synthesized by dip coating deposition of sol-gel TiO_2 using an optimized T-mixer setup. Material characterization and hydraulic properties were carried out to determine the influence of undoped and doped TiO_2 coatings on permeate flux using deionized (DI) water and acid orange 7 (AO7). The photowetting process in DI water was investigated in the absence of AO7. The filter performance was evaluated using the removal efficiency and cumulative removal of AO7 using a medium mercury pressure lamp (λ = 365 nm), a commonly used artificial UV light source in photocatalytic reactors. The study highlights the optimization of doping parameters, such as the type of dopant (N or B) and concentration, on TiO_2 filter using solely UVA irradiation to assess improvements in removal compared to undoped TiO_2.

2. Experimental section

2.1. Materials

Titanium isopropoxide (TTIP, 97 %), urea, boric acid, and isopropanol (IPA, HPLC grade) were used as synthesis materials and obtained from Sigma-Aldrich. Acid orange 7 (AO7, > 85 %) was also obtained from Sigma-Aldrich and used as a model pollutant for filtration experiments. Commercial α-Al_2O_3 porous ceramic discs (diameter: 50 mm, thickness: 6 mm) with a pore size of 1.4 μm were purchased from Coors Tek, Inc. Quartz fiber filters (Type A/G, particle retention = 1.0 μm) were obtained from Pall Corporation and were used as substrates for TiO_2 sol-gel deposition.

2.2. Preparation of membranes

Preparation of the different kind of membranes is adapted elsewhere [30]. TiO_2 quartz fiber filters (TQFF) were prepared using a sol-gel method using a T-mixer setup (See Fig. S1 in Supplementary Information). Undoped TiO_2 nanoparticles were synthesized by mixing two solutions: (A) ultra water/IPA and (B) TTIP/IPA (C_{Ti} = 0.126 M) at 20 °C. Equal volumes of reactant solutions (100 mL) at 20 °C were pumped into a static T-mixer using two peristaltic pumps at a flow rate of 0.6 L min^{-1} [26]. The hydrolysis ratio was C_w/C_{Ti} = 2.1. Doped nanoparticles were prepared using the aforementioned procedure with the addition of different amounts of urea (C_N/C_{Ti} = 3, 5, and 7×10^{-2}) and boric acid (C_B/C_{Ti} = 3, 5, and 7×10^{-2}) for N-doped and B-doped nanoparticles, respectively. The dopant compounds were added to solution (A) prior to injection with solution (B) into the T-mixer.

The particles were immobilized during their period of relative stability, $t < t_{induction}$ [51]. QFF were washed with sulphuric acid (98%) for 1 h and then rinsed with ultrapure water, followed by drying at 70 °C overnight. The supports were submerged for 90 s in the TiO_2 nanoparticle suspension at a withdrawal speed of 2 mm min^{-1} using a dip-coating apparatus (MTI Corporation, PTL-MMBO1); this process was repeated 6 times for adequate coating thickness and subsequently dried at 70 °C overnight. After drying, calcination was conducted using a ramp rate of 2 °C min^{-1} to a final temperature of 400 °C. The coated filters were washed in ultra water to remove any excess non-reacted and loose nanoparticles from the filter.

For N-TiO_2/QFF (NTQFF), the following abbreviations are used to denote samples at C_N/C_{Ti} concentration ratios of 3, 5, and 7×10^{-2}, respectively: $NTQFF_3$, $NTQFF_5$, and $NTQFF_7$. Similarly, for B-TiO_2/QF (BTQFF), the following abbreviations were used to denote samples at C_B/C_{Ti} concentration ratios of 3, 5, and 7×10^{-2}, respectively: $BTQFF_3$, $BTQFF_5$, and $BTQFF_7$.

2.3. Analytical procedures

2.3.1. Materials characterization

The phase and microstructure of the thin films were evaluated using X-ray diffraction (XRD), Raman spectroscopy, and scanning electron microscopy (SEM). The morphology of thin films was characterized using a ZEISS LEO 1550 FE-SEM at an accelerating voltage of 10 kV. The crystal phase was determined using an Inel powder X-ray Diffractometer (XRD) with Cu-Kα_1 radiation (λ = 1.5406Å and a position sensitive detector. The tube current was set at 30 mA and the generator voltage was at 30 kV. Raman spectroscopy was conducted using a Renishaw Ramanscope equipped with a He-Ne laser (λ = 633 nm, 10 mW, Melles Griot) and a diffraction grating (1800 lines mm^{-1}). The spatial resolution of the spectrometer was less than 1 cm^{-1}.

X-ray photoelectron spectroscopy (XPS) was conducted to determine the chemical composition and chemical bonds. A Thermo ESCALAB 250 instrument configured with an $Al_{K\alpha}$ X-ray source (1486.6 eV, 150 W), a hemispherical analyzer (150 mm radius), and an analysis chamber was used. Data was collected with pass energy of 20 eV for the core-shell spectra and 50 eV for the survey spectrum. The takeoff angle, defined as the angle between the substrate normal and the detector, was fixed at 0°. Non-monochromated $Al_{K\alpha}$ twin anode was

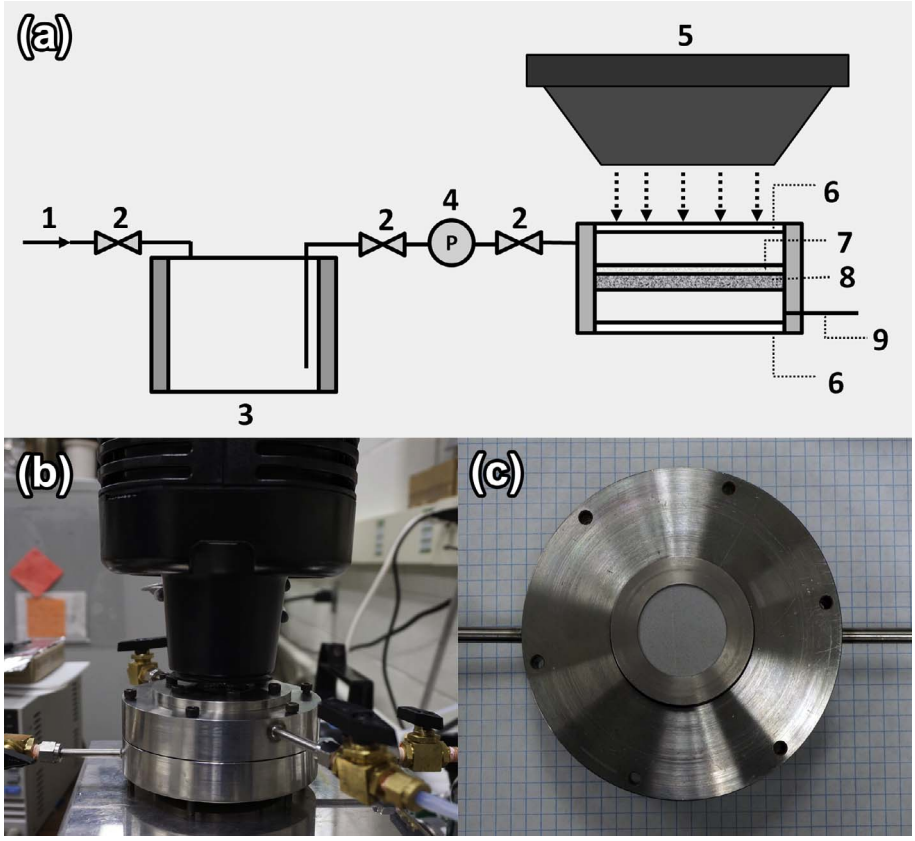

Fig. 1. (a) Schematic of photocatalytic membrane reactor (PMR) setup containing (1) compressed air line, (2) valve, (3) pressurized feed tank, (4) pressure gauge, (5) UV irradiation source, (6) quartz window, (7) membrane, (8) α-Al_2O_3 porous support, (9) permeate outlet; (b) UV light emission from medium-pressure mercury lamp with collimating funnel targeting PMR quartz window; and (c) TiO_2 membrane on porous support in a stainless steel housing.

used to reduce charging in some samples. Ti_{2p}, O_{1s}, N_{1s}, and B_{1s} peaks were analyzed and their peaks were deconvoluted.

2.3.2. Photocatalytic membrane reactor setup and experiments

The photocatalytic membrane reactor (PMR) test setup is shown in Fig. 1. The permeate flux, transmembrane pressures and analyte concentration were measured. The setup (Fig. 1) is comprised of a compressed air line, pressurized feed tank, pressure gauge, UV irradiation source, and PMR module. The designed PMR module was made out of stainless steel and contains an inlet and outlet with a quartz window to transmit a light source through the enclosure and onto the membrane. Polyethylene tubing (outer diameter of 5/16″ and inner diameter of 3/16″) was used as connections. Medium pressure mercury lamp (MPM, UVP Blak-Ray B-100SP, 100 W) was used as the UV irradiation source and the beam was collimated using an accessory funnel with a height of 10.2 cm (4″). The effective quartz window and membrane illumination area was 38.1 cm (1.5″). A porous support disc was used in conjunction with the photocatalytic membrane to add enough resistance for an optimum flow rate for testing. A silicon (Si) photodiode (Thorlabs, PM-100USB) was used to measure the power density at a reference point 2 cm from the collimating funnel of the MPM lamp; the power density was adjusted to 12.0 mW cm^{-2} at $\lambda = 365$ nm at this reference point.

In order to evaluate the membrane permeate properties, the water permeability and flux under dark and UV conditions were tested. The performance of various undoped and doped membranes were evaluated using AO7 azo dye (See Table S1 for properties of the dye in Supplementary Information). Dead-end filtration was carried out to evaluate the combined photocatalytic and separation performance using a test solution of 2 mg L^{-1} AO7 in a 5 L feed tank. Membranes and porous alumina supports were immersed in AO7 solution for 1 h prior to the experiment to eliminate the adsorption effects of AO7 dye. During the experiment, the MPM lamp was switched on for 1 h, followed by 1 h of filtration in the dark. The transmembrane pressure was fixed at 0.5 bar. After single pass filtration, the treated water was collected in the bottom chamber where it could be analyzed. The concentration of AO7 was determined using a UV–Vis spectrometer (Shimadzu UV-2501 PC) from a range of 200 nm to 800 nm. The peak height of the AO7 molecule at the 485 nm peak was used to determine the concentration from prepared calibration curves in the linear range. Adsorption tests were replicated in triplicates.

3. Results and discussion

3.1. Membrane material characteristics

Pure and doped TiO_2 were immobilized onto a QFF during the induction period of the sol-gel reaction. These TiO_2/QF filters were characterized using SEM, XRD, and Raman spectroscopy. Uncoated QFF (Fig. 2a) consisted of fibers less than 2 μm in diameter, with lengths ranging from 10 to 100 μm. The coated QFF consisted of thin layers of TiO_2 as seen in Fig. 2. The TiO_2 agglomerates are deposited directly on the QF, allowing for a porous network structure and high surface area. Pristine TiO_2 sol-gel and B-TiO_2 appeared homogeneous (Fig. 2b and d) compared to N-TiO_2 in which nanoparticles agglomerated and formed clusters (Fig. 2c). These agglomerates were also observed by Kadam et al. when they doped TiO_2 nanoparticles with nitrogen [52].

The bandgap energy – the minimum energy for the generation of electron-hole pairs – was determined from diffuse reflectance spectra of the membranes. The diffuse reflectance spectrum was converted into a Tauc plot, $[hvF(R)]^{1/n}$ vs. hv, where h is the Planck's constant, v is the frequency, R is the reflectance, n is a constant related to the nature of the sample transition, and $F(R)$ is the Kubelka-Munk function, given by:

$$F(R) = \frac{(1-R)^2}{2R} \tag{4}$$

The value of n is 2 because TiO_2 is an indirect bandgap semiconductor [53,54]. The bandgap was estimated as the intercept between x-axis and the tangent line of the inflection point (See Fig. S2 in

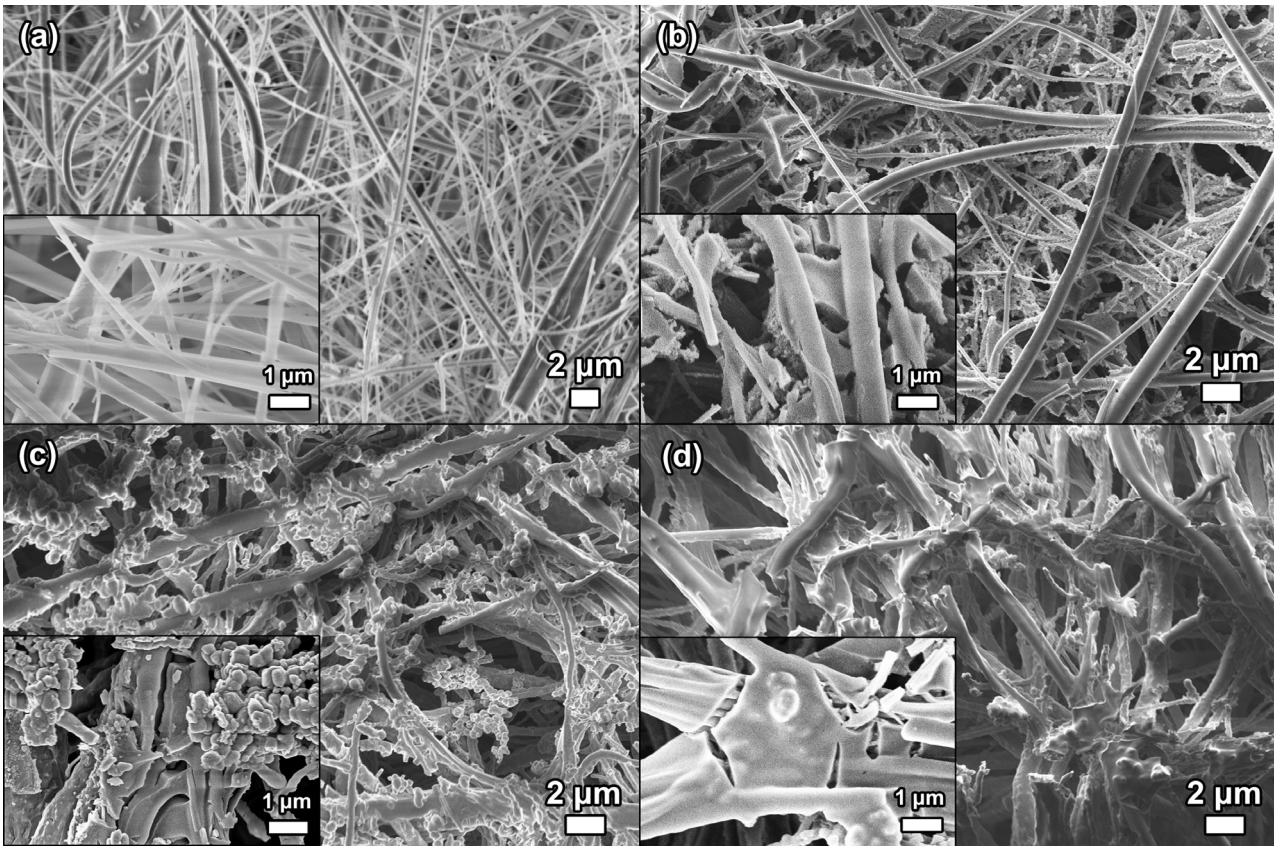

Fig. 2. SEM images of the following filters: (a) QFF (b) TQFF, (c) $NTQFF_5$, and (d) $BTQFF_5$.

Supplementary Information). The optical bandgap of pure TiO_2 and B-TiO_2 was 3.20 eV; there is no significant difference in the bandgap energy of these two materials, which is in agreement with the reported results [55]. The bandgap of N-TiO_2 was narrowed to 3.15 eV, which is consistent with literature [45–47], and there exists a wavelength range that can excite electrons in N-TiO_2 that are not permissible in undoped TiO_2 or B-TiO_2.

The X-ray diffraction patterns of TiO_2, B-TiO_2, and N-TiO_2 produced by the sol–gel process and heat treated at 400 °C are shown in comparison with commercial P25 Aeroxide™ (Fig. 3). The doped and undoped TiO_2 diffraction patterns show characteristic anatase peaks of (1 0 1), (0 0 4), (2 0 0), (1 0 5), (2 1 1), (2 0 4), (1 1 6), (2 2 0), and (2 1 5) planes. The P25 Aeroxide™ contains anatase and a minor amount of rutile, represented by the (1 1 0), (1 0 1), and (1 1 1) diffraction peaks. N and B doping conducted from a range of 3×10^{-2} to 7×10^{-2} dopant/Ti concentration ratio did not affect the crystal phase of the samples, nor produced other crystalline diffraction peaks. This is either because dopants are highly dispersed into the TiO_2 structure, or the XRD is not sensitive enough to detect crystalline peaks containing these dopants [56–59]. This suggests that dopants may have moved into substitutional/interstitial sites in the crystal structure rather than reacting with TiO_2.

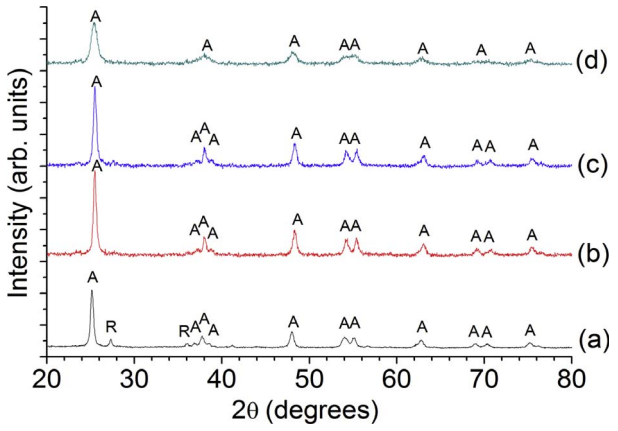

Fig. 3. X-ray diffraction patterns of (a) P25 Aeroxide™, (b) TiO_2 sol-gel, (c) N-doped TiO_2 and (d) B-doped TiO_2 powders. Anatase (A) and rutile (R) phases are labelled.

XPS was used to determine the presence of nitrogen or boron incorporated into the TiO_2 photocatalyst. Table 1 lists the binding energies of peaks found in Ti_{2p}, O_{1s}, N_{1s}, and B_{1s} regions which were deconvoluted (See Fig. S3 in Supplementary Information). All of the TiO_2 samples exhibited $Ti_{2p3/2}$ and $Ti_{2p1/2}$ peaks at 459.5 eV and 465.2 eV, respectively, which are consistent with values reported in literature [15,60]. The O_{1s} peaks of undoped, N-doped, and B-doped TiO_2 possessed of an asymmetric peak that was deconvoluted into two peaks with binding energy values of 530.6 eV and 532.0 eV. Furthermore, the broader O1 s peaks was apparent in B-doped TiO_2 sample compared to the undoped and N-doped TiO_2 samples suggesting greater surface defects [61].

N-doped TiO_2 exhibited a 400.6 eV peak in the $N_{1\,s}$ spectra, signifying the presence of interstitial nitrogen, N—O bonds in the photocatalyst matrix, or NH_4^+ species [55,62]. It was found that interstitial nitrogen has no significant shift in conduction or valence bands of TiO_2, but the anti-bonding π^* N—O orbital between the TiO_2 valence and conduction bands facilitating visible light absorption which benefits increases efficiency at the visible light range and hence the reaction rate for treatment processes using solar energy [34]. B-doped TiO_2 exhibited a peak at 192.9 eV associated with the B-O-B bonds in B_2O_3 [58,63]. The addition of boron by interstitial B-doping or formation of B_2O_3 on TiO_2 particle have unclear effects in photocatalytic activity in the treatment of various compounds [58,63].

Table 1
XPS peaks for undoped, N-doped, and B-doped TiO_2 powders.

Sample	Binding Energy (eV) and Percentage of Integrated XPS region spectra					
	Ti_{2p} region		O_{1s} region		N_{1s} region	B_{1s} region
	$Ti_{2p1/2}$	$Ti_{2p3/2}$	O_{1s}	O_{1s}	N_{1s}	B_{1s}
Undoped TiO_2	465.19 (32.03%)	459.49 (67.97%)	530.72 (85.52%)	532.2 (14.48%)		
N-doped TiO_2	465.16 (32.74%)	459.46 (67.26%)	530.71 (86.06%)	532.1 (13.94%)	400.62 (100%)	
B-doped TiO_2	465.21 (31.42%)	459.55 (68.58%)	530.77 (60.45%)	531.52 (39.55%)		192.9 (100%)

3.2. Water permeability experiments

The permeate flux was obtained from the measurements of flow rate at the outlet of the PMR module as shown in Fig. 1a. The permeate flux is defined by Darcy's law:

$$J_P = \frac{Q}{A} = \frac{L_P}{\mu}\Delta P = \frac{\Delta P}{\mu R_m} \quad (5)$$

where J_p is the flux density (m s^{-1}), Q is the flow rate (m^3 s^{-1}), A is the filtration area, L_p is the hydraulic permeability of the membrane (m), μ is the dynamic viscosity of the solvent used (Pa s), ΔP is the transmembrane pressure (Pa), and R_m is the hydraulic resistance of the membrane [64]. The hydraulic permeability (L_p) of the fiber filters depend on intrinsic characteristics of the membrane such as size distribution, thickness and hydrophilic nature. The permeability of all membranes was obtained from flux vs. transmembrane pressure plots (See Fig. S4). The total membrane resistance can be determined by the sum of the contributions of each component in the membrane stack, given by:

$$R_m = R_p + R_f + R_c \quad (6)$$

where R_p, R_f, and R_c are the hydraulic resistances of the porous support, QFF, and TiO_2 coating, respectively. The undoped, N-doped, and B-doped TiO_2 membrane resistances are shown in Fig. 4. The addition of TiO_2 coating decreases the water permeability and increases resistance. In the case of TQFF and $NTQFF_5$, there is a 9% and 29% decrease, respectively in water permeability. This phenomenon was also observed elsewhere [28,31], and is due to increased thickness and pore size reduction after TiO_2 deposition. Doped TiO_2 samples have higher hydraulic resistances due to increased deposition of N-doped and B-doped TiO_2 onto the surface of the QFF, albeit different surface morphologies, as seen in the SEM images (Fig. 2).

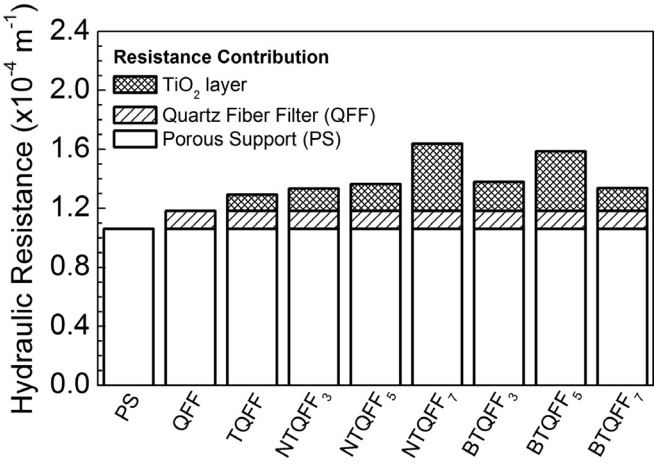

Fig. 4. Hydraulic resistances of QFF, TQFF, NTQFF, and BTQFF membranes.

3.3. Photowetting processes of TiO_2 filters

The addition of a TiO_2 layer introduces an effect called photowetting, in which the surface wettability of a substrate can be changed by light stimuli. Wang et al. observed amphiphilic surfaces when conducting contact angle measurements, in which a TiO_2 surface under dark formed water droplets that varied from 15° to 72°, increasing in hydrophobicity as a function of time in darkness. Upon UV illumination, the contact angle changed to 0° [65]. The contact angle, θ, of a TiO_2 film under aqueous conditions generally decreases after UV exposure. This can be modelled using an exponential function [66]:

$$\theta = \theta_0 e^{-k_{UV} t} \quad (7)$$

where k_{UV} is the rate constant. The k_{UV} value from other sources that use TiO_2 films was around 0.15–0.16 min^{-1} [66,67]. The function was plotted in Fig. 5a to visualize contact angle decrease of TiO_2 on a relatively flat surface. As in the case of water, it has been proven that the same process can be applied to organic solvents and is independent of photocatalytic activities [37,65,68].

The normalized permeate flux of TQFF using DI water was compared to QFF under two conditions (Fig. 5b): (i) 2 h dark and (ii) 1 h dark with 1 h UV. In the case of 2 h dark condition, the flux steadily decreased by around 15% of its initial value for both QFF and TQFF towards equilibrium conditions. When UV light was introduced, the flux increased by about 12% initially using TQFF, and did not change when using naked QFF. The increased flux under illumination and decrease in flux in dark conditions using TQFF demonstrates the photowetting effect in TiO_2 because the increase in hydrophilicity decreases the membrane resistance and water passes through the membrane easily in comparison to more hydrophobic materials resulting in increased flux [69,70]. QFF also did not show a sudden increase in flux after illumination indicating that it is not irradiation of UV light alone that contributes to increased flux, but rather a material property of TiO_2 in TQFF as depicted in Fig. 5a.

The flux measurements were further carried out under dark and UV illumination conditions as a function of time for NTQFF and BTQFF samples (Fig. 6). Filtration was carried out in the dark for 1 h, followed by UV illumination in the next hour. Fig. 6 depicts the normalized flux of TQFF, NTQFF, and BTQFF. Under UV illumination for 10 min and 60 min, there was an increase of 12% and 14% increase in flux for the TQFF compared to its baseline under dark conditions (at time point 60 min). This may be due to TiO_2 photowetting effect. In the case of NTQFF samples (Fig. 6a), the flux increased under UV illumination initially (at time point 70 min) by 0%, 13%, and 7%, respectively. After 1 h of UV illumination, the flux decreased by 7% for $NTQFF_3$ and increased by 20% and 7% for $NTQFF_5$ and $NTQFF_7$, respectively. TQFF, $NTQFF_5$, and $NTQFF_7$ all demonstrated an increase in DI water flux when using a UVA radiation source. In the case of BTQFF samples (Fig. 6b), at doping concentration ratios of C_B/C_{Ti} = 3, 5, and 7×10^{-2}, the flux did not increase under UVA illumination at any point.

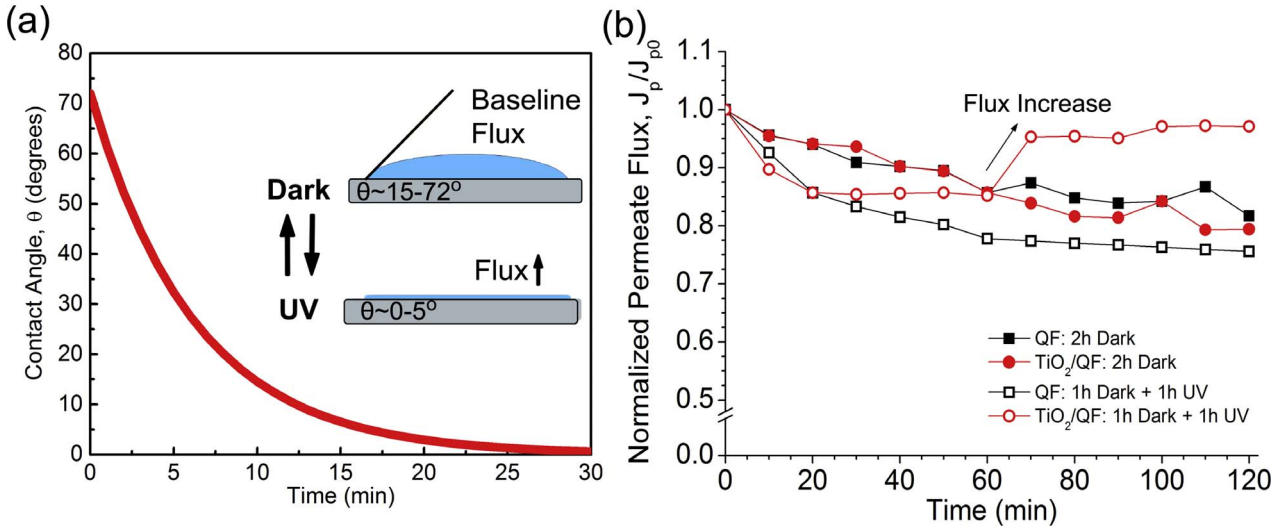

Fig. 5. (a) Schematic of photowetting effect on TiO_2 surface; and (b) Normalized Permeate QFF and TQFF membranes.

3.4. Removal of AO7 using photocatalytic membrane filtration

AO7 was chosen as a compound of interest for the filtration through PMR because it is a non-biodegradable dye and any direct biological treatments are ineffective in removing this organic compound; however it can be removed through oxidation processes using TiO_2 in conjunction with a UV source or through filtration. In this study, the adsorption, permeate flux, and removal efficiency were measured and analyzed for QFF, TQFF, NTQFF, and BTQFF. The water purification experiments were performed using photocatalytic filtration treatment of AO7 solutions with concentration of 2 mg L^{-1} (5.7×10^{-6} mol L^{-1}).

3.4.1. AO7 adsorption on filters

All undoped and doped TQFFs and α-alumina porous supports were immersed in 50 mL of the solution of AO7 at 2 mg L^{-1} for 1 h under darkness and stirring to reach the adsorption equilibrium. The following equation was used to calculate the percentage of the initial concentration of dye adsorbed on the membrane:

$$\%adsorption = \frac{(C_o - C_{eq})}{C_o} \quad (8)$$

where C_o and C_{eq} are the AO7 concentration at the initial and the equilibrium state, respectively. The AO7 adsorption of the membranes was quantified and shown in Fig. 7. Using nitrogen as a dopant, the adsorption of AO7 was higher than with undoped TiO_2. This may be due to the film morphology in which N-TiO_2 sol-gel nanoparticles deposited a greater number of TiO_2 agglomerates on the NTQFF than TQFF, increasing the surface area and thus the total adsorption of AO7. Increased B-doping of BTQFF reduced the adsorption because of its

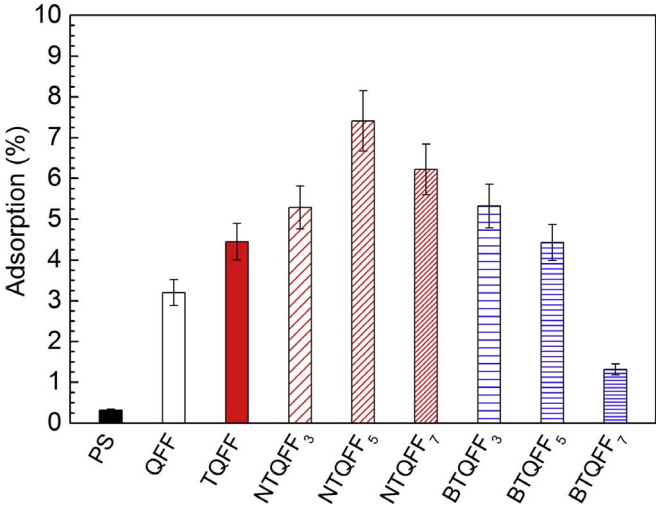

Fig. 7. Percentage of initial concentration of dye adsorbed on the surface of the porous support, bare quartz fiber filter (QFF), and doped and undoped TiO_2/QFF.

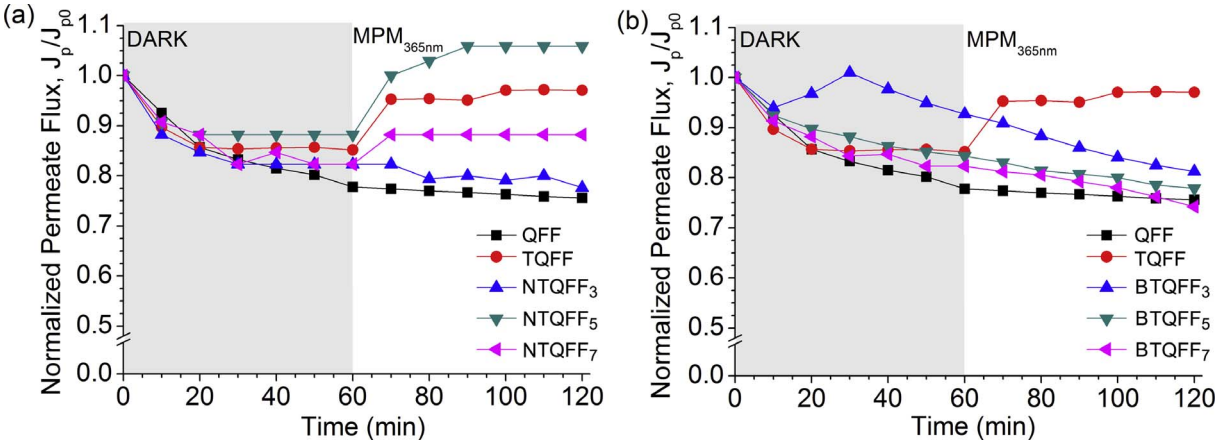

Fig. 6. Permeate flux of a) NTQFF and b) BTQFF using DI water under dark and UV illumination period.

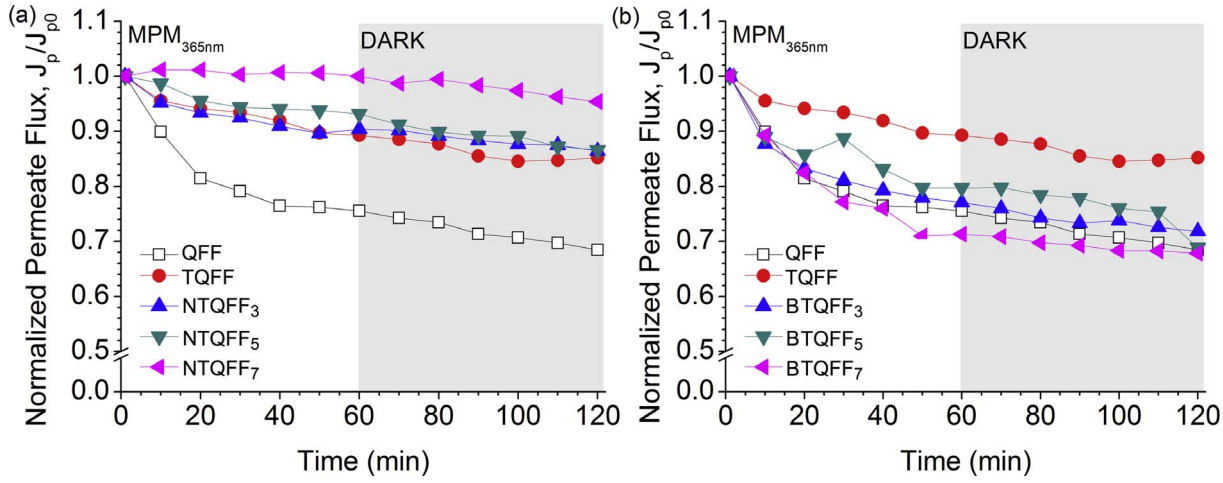

Fig. 8. Permeate flux of a) NTQFF and b) BTQFF membranes using AO7 (2 mg L^{-1}) in water under UV and dark conditions.

"smooth" film morphology (Fig. 2d), in comparison to the high surface agglomeration of TiO_2 particulates on NTQFF (Fig. 2c), which results in a lower surface area for adsorption.

3.4.2. Permeate flux using AO7 under UV and dark conditions

After equilibrium was achieved, filtration of dye solution was carried out using the PMR setup (Fig. 1). A solution of AO7 (2 mg L^{-1}) was fed into the PMR module for 2 h, followed by 1 h under UV then 1 h in the dark, and the permeate flux was measured in Fig. 8. The flux through the filters in AO7 solution was lower than DI water, which is attributed to dye molecules accumulating on the membrane surface forming a cake layer and increasing the membrane resistance [27].

The permeate flux of the uncoated membranes decreased continuously to 32% of its initial value through 2 h of the experiment and UV irradiation had no effect on the permeate flux. The permeate flux decreased less using TQFF and NTQFF than QFF under UV irradiation. The minimal decrease in flux for TQFF and NTQFF samples compared to QFF is due to an increase in wettability as mentioned and antifouling properties of TiO_2 caused by photocatalytic degradation on the membrane surface [14,27,30]. The contribution of photocatalysis and photowetting processes is not easily understood as they both occur under light processes and quantifying the contribution of each is not in the scope of this study.

The flux of all membranes decreased slightly after switching to dark conditions after 1 h of UV irradiation. The contact angle does not change rapidly after UV irradiation is removed so the hydrophilicity and flux would not significantly changed over 1 h in the dark [71]. This phenomenon was shown by Lee et al. in which they found that when switching from the hydrophobic to hydrophilic state (turning the UV source on) the contact angle change occurs in the order of minutes; whereas switching from the hydrophilic state to the hydrophobic state (turning the UV source off), occurs in the order of days [71]. In the case of BTQFF, there were no significant changes in normalized permeate flux compared to QFF.

3.4.3. Removal of AO7 under UV and dark conditions

The percentage (Fig. 9a and b) and cumulative (Fig. 9c and d) removal of AO7 were conducted under 1 h irradiation, followed by 1 h dark condition using undoped and doped filters. The percentage removal and cumulative removal are defined as:

$$\text{Percentage Removal} = \frac{C_o - C_t}{C_t} \times 100(\%) \quad (9)$$

$$\text{Cumulative Removal} = \frac{\sum_t (C_o - C_t) \times V_t}{M \times A} (\text{molm}^{-2}) \quad (10)$$

where C_o is the initial concentration (mol L^{-1}), C_t is the concentration at time t (mol L^{-1}), V_t is the total volume filtered (L), M is the molar mass (g mol^{-1}), and A is the filtration area (m^2). The percentage removal does not take into account the hydraulic resistance of the membranes, and only gives the permeate concentration at specific time with respect to the inlet concentration. However, the cumulative removal considers the permeate flux, or the volume the membrane has filtered, and area of the membrane.

The percentage removal of $NTQFF_3$ and $NTQFF_7$ was compared to TQFF and QFF. The results indicated that the removal of AO7 using NTQFF was higher than QFF and was dependent on the concentration of the dopant. After 1 h of UV irradiation, $NTQFF_5$ and $NTQFF_7$ removed 10% and 55%, respectively, more on a percentage basis than TQFF. However $NTQFF_3$ removed 45% less than the TQFF. Under dark conditions, the removal percentage lowers as a function of time, whereas TQFF stays constant over 1 h. This is caused by the greater photocatalytic activity in NTQFF than TQFF. There is also an increased hydraulic resistance in doped TiO_2 filters (Fig. 8). This observation suggests that because of the lowered flux, the volume filtered and the cumulative removal are generally lower compared to undoped TiO_2 filters. The $NTQFF_7$ had a greater cumulative removal under UV conditions than TQFF, but the removal rate over time decreased under dark conditions. The decrease in removal rate was also apparent for $NTQFF_3$ and $NTQFF_5$ when switching from UV conditions to dark conditions. The change in rate may be due to the wetting properties in which the contact angle decreases exponentially as in Eq. (7).

The higher photoactivity of the NTQFF compared to TQFF may also due to the fact that N-doping is accompanied by oxygen vacancy formation. The formation of the oxygen vacancies on the surface favors the adsorption of water molecules and thus increases the amount of hydroxyl radicals which are responsible of the degradation of the pollutant molecule.

$BTQFF_3$, and $BTQFF_7$ had a 70% and 45% lower AO7 percent removal compared to TQFF, respectively. However, $BTQFF_5$ demonstrated a 20% increase in percent removal compared to TQFF. There was no difference in dye removal when comparing under UV irradiation and dark conditions as revealed by the water flux measurements in Fig. 8b, in which no apparent changes in flux were observed. Boron was shown to be a poor dopant for TiO_2 photocatalysis compared to undoped TiO_2 sources under UVA radiation sources [72,73]. Additionally, the cumulative removal of AO7 using $BTQFF_3$ and $BTQFF_7$ was lower than that of TQFF. The lower cumulative removal was due to higher hydraulic resistance as in the NTQFF samples except for $BTQFF_7$, which demonstrated higher cumulative removal than other B-doped filters.

Higher doping concentrations, such as in $BTQFF_7$, may also decrease photoreactivity and hence removal and may be attributed to the

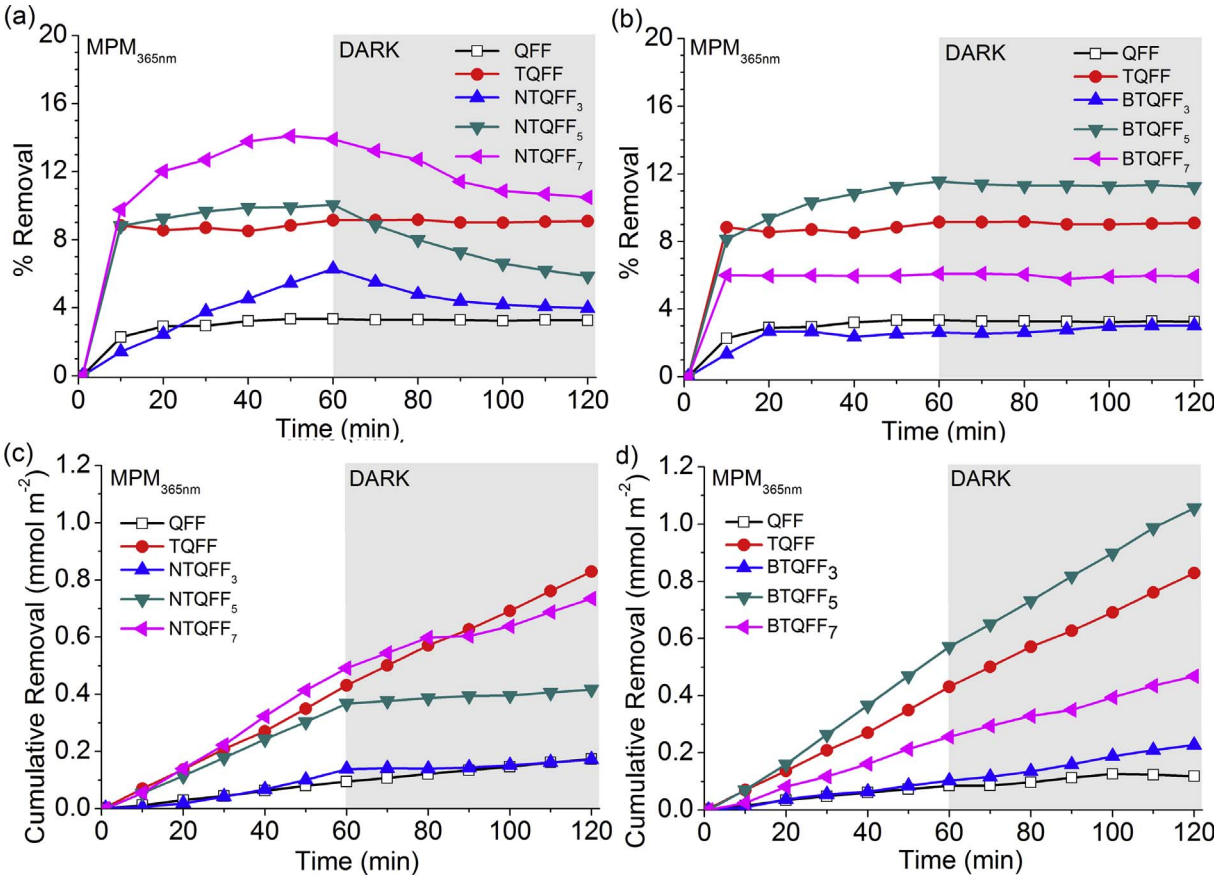

Fig. 9. Percentage (a, b) and cumulative removal (c, d) of AO7 in (a, c) NTQFF and (b, d) BTQFF samples.

exponential increase in recombination as a function of the dopant concentration because the average distance between trap sites decreases with increasing the number of dopants confined within a particle. At lower concentrations below an optimal doping concentration, photoreactivity increases with increasing dopant concentration because there are available trapping sites in the crystal structure.

The NTQFF membranes may be further improved using solar sources as the medium pressure mercury lamp has a peak wavelength of 365 nm and this does not extend to the visible light region. The application of solar light in the form of natural sunlight or xenon illumination may be used to improve N-TiO_2, however, this is out of scope for this study. Doping with nitrogen has been shown in literature to improve the photoactivity under visible light conditions (400–500 nm) [74].

The removal rates under UV in different studies are presented in Table 2. The various differences in removal rates are due to structure/morphology of the substrates, chemical composition, feed pollutant solution concentration, and different reactor setups. The removal rates in this study are on the same order of magnitude as the two other studies analyzed [75]. Only $NTQFF_7$ had a removal rate that was one order magnitude greater than any of the other substrates compared.

4. Conclusions

Photocatalytic quartz fiber filters were modified using sol-gel processes. The pore size and TiO_2 deposits were controlled by the sol properties, immersion time, and thermal treatment temperature and duration. TiO_2 coatings on quartz filters were determined to be anatase for both undoped and doped TiO_2 filters via XRD and Raman analysis. Coupling adsorption, photowetting, photocatalysis, and membrane filtration into a PMR by adding TiO_2 sol-gel coating on QFF increased the flux and improved the removal rate of dissolved organic matter compared to uncoated QFF. It was discovered that the flux did not drop immediately after UVA radiation was removed during the AO7 filtration process due to the photowetting effect. NTQFF and TQFF demonstrated increased permeate flux using DI water and AO7 under dark and UV illumination; whereas the flux in BTQFF and QFF did not improve after UV irradiation was introduced. Higher doping concentrations generally produced better membrane removal properties than the lowest dopant concentration used. For example, the percentage and cumulative removal of AO7 was favourable using $NTQFF_7$ and $BTQFF_5$ compared to TQFF. Only NTQFF samples were able to show distinct photohydrophylic activity compared to TQFF and BTQFF. The lack of distinct photohydrophylic activity may be due a combination of lower

Table 2
Comparison of different degradation rates of TiO_2 membranes in AO7 solution under UV irradiation.

Source	This study			Mendret [75]	Bosc [75]
Substrate	TQFF	$NTQFF_3$, $NTQFF_5$, $NTQFF_7$	$BTQFF_3$, $BTQFF_5$, $BTQFF_7$	TiO_2/Al_2O_3	TiO_2/Al_2O_3
Filtration type	Dead-end			Dead-end	Cross-flow
[AO7] (mol L^{-1})	5.71×10^{-6}			2.85×10^{-5}	2.50×10^{-5}
Removal rate (mol $L^{-1} h^{-1}$)	4.63×10^{-6}	3.54, 8.69, 76.0 $\times 10^{-6}$	1.18, 5.61, 1.45 $\times 10^{-6}$	2.85×10^{-6}	3.53×10^{-6}

reactivity and high fluxes. Additional studies on the effect of sunlight or a visible light source is useful in further determining the efficacy of doped-membranes in PMR.

Acknowledgements

The authors acknowledge financial support from the Natural Sciences and Engineering Research Council of Canada through a strategic project grant (STPGP-494554-2016), the Canadian Water Network Innovation Technologies for Water Treatment Program, and the Canadian Research Chair Program.

Appendix A. Supplementary data

Supplementary data associated with this article can be found, in the online version, at http://dx.doi.org/10.1016/j.cej.2017.07.141.

References

[1] C.A.K. Gouvêa, F. Wypych, S.G. Moraes, N. Durán, N. Nagata, P. Peralta-Zamora, Semiconductor-assisted photocatalytic degradation of reactive dyes in aqueous solution, Chemosphere 40 (2000) 433–440, http://dx.doi.org/10.1016/S0045-6535(99)00313-6.

[2] P. Cooper, Removing colour from dyehouse waste waters—a critical review of technology available, J. Soc. Dye. Colour 3 (1993) 97–100, http://dx.doi.org/10.1111/j.1478-4408.1993.tb01536.x.

[3] A.L. Ahmad, M.R. Othman, H. Mukhtar, H 2 separation from binary gas mixture using coated alumina – titania membrane by sol – gel technique at high-temperature region, Int. J. Hydrogen Energy 29 (2004) 817–828, http://dx.doi.org/10.1016/j.ijhydene.2003.10.003.

[4] I. Voigt, G. Fischer, P. Puhlfu, M. Schleifenheimer, M. Stahn, TiO 2 -NF-membranes on capillary supports, Sep. Purif. Technol. 32 (2003) 87–91, http://dx.doi.org/10.1016/S1383-5866(03)00064-9.

[5] R.J. Davis, J.L. Gainer, G.O. Neal, I. Wu, J. Davis, Photocatalytic decolorization of wastewater dyes, Water Environ. Res. 66 (1994) 50–53, http://dx.doi.org/10.2175/WER.66.1.8.

[6] M. Oturan, N. Oturan, M. Edelahi, Oxidative degradation of herbicide diuron in aqueous medium by Fenton's reaction based advanced oxidation processes, Chem. Eng. J. 171 (1) (2011) 127–135, http://dx.doi.org/10.1016/j.cej.2011.03.072.

[7] M. Hussain, R. Ceccarelli, D.L. Marchisio, D. Fino, N. Russo, F. Geobaldo, Synthesis, characterization, and photocatalytic application of novel TiO2 nanoparticles, Chem. Eng. J. 157 (2010) 45–51, http://dx.doi.org/10.1016/j.cej.2009.10.043.

[8] A. Mills, S. Le Hunte, An overview of semiconductor photocatalysis, J. Photochem. Photobiol. A Chem. 108 (1997) 1–35, http://dx.doi.org/10.1016/S1010-6030(97)00118-4.

[9] M.A. Henderson, A surface science perspective on photocatalysis, Surf. Sci. Rep. 66 (2011) 185–297, http://dx.doi.org/10.1016/j.surfrep.2011.01.001.

[10] M. Faisal, M. Abu, A. Khan, K. Umar, M. Muneer, Photochemical reactions of 2,4-dichloroaniline and 4-nitroanisole in aqueous suspension of titanium dioxide, Sci. Adv. Mater. 3 (2011) 269–275, http://dx.doi.org/10.1166/sam.2011.1153.

[11] R. Liang, A. Hu, W. Li, Y.N. Zhou, Enhanced degradation of persistent pharmaceuticals found in wastewater treatment effluents using TiO2 nanobelt photocatalysts, J. Nanoparticle Res. 15 (2013) 1990, http://dx.doi.org/10.1007/s11051-013-1990-x.

[12] K. Tennakone, C.T.K. Tilakaratne, I.R.M. Kottegoda, Photocatalytic degradation of organic contaminants in water with TiO2 supported on polythene films, J. Photochem. Photobiol. A Chem. 87 (1995) 177–179, http://dx.doi.org/10.1016/1010-6030(94)03980-9.

[13] M.G. Antoniou, P. a. Nicolaou, J. a. Shoemaker, A. a. de la Cruz, D.D. Dionysiou, Impact of the morphological properties of thin TiO2 photocatalytic films on the detoxification of water contaminated with the cyanotoxin, microcystin-LR, Appl. Catal. B Environ. 91 (2009) 165–173, http://dx.doi.org/10.1016/j.apcatb.2009.05.020.

[14] H. Choi, E. Stathatos, D.D. Dionysiou, Photocatalytic TiO2 films and membranes for the development of efficient wastewater treatment and reuse systems, Desalination. 202 (2007) 199–206, http://dx.doi.org/10.1016/j.desal.2005.12.055.

[15] R. Azouani, A. Michau, K. Hassouni, K. Chhor, J.-F. Bocquet, J.-L. Vignes, A. Kanaev, Elaboration of pure and doped TiO2 nanoparticles in sol–gel reactor with turbulent micromixing: application to nanocoatings and photocatalysis, Chem. Eng. Res. Des. 88 (2010) 1123–1130, http://dx.doi.org/10.1016/j.cherd.2009.10.001.

[16] P. Pucher, M. Benmami, R. Azouani, G. Krammer, K. Chhor, J.-F. Bocquet, A.V. Kanaev, Nano-TiO2 sols immobilized on porous silica as new efficient photocatalyst, Appl. Catal. A Gen. 332 (2007) 297–303, http://dx.doi.org/10.1016/j.apcata.2007.08.031.

[17] R. Molinari, A. Caruso, T. Poerio, Direct benzene conversion to phenol in a hybrid photocatalytic membrane reactor, Catal. Today. 144 (2009) 81–86, http://dx.doi.org/10.1016/j.cattod.2009.02.034.

[18] H. Zhang, X. Quan, S. Chen, H. Zhao, Y. Zhao, Fabrication of photocatalytic membrane and evaluation its efficiency in removal of organic pollutants from water, Sep. Purif. Technol. 50 (2006) 147–155, http://dx.doi.org/10.1016/j.seppur.2005.11.018.

[19] M. Benmami, K. Chhor, A.V. Kanaev, High photocatalytic activity of monolayer nanocoatings prepared from non-crystalline titanium oxide sol nanoparticles, Chem. Phys. Lett. 422 (2006) 552–557, http://dx.doi.org/10.1016/j.cplett.2006.03.001.

[20] A. Fernández, G. Lassaletta, V.M. Jiménez, A. Justo, A.R. González-Elipe, J.-M. Herrmann, H. Tahiri, Y. Ait-Ichou, Preparation and characterization of TiO2 photocatalysts supported on various rigid supports (glass, quartz and stainless steel). Comparative studies of photocatalytic activity in water purification, Appl. Catal. B Environ. 7 (1995) 49–63, http://dx.doi.org/10.1016/0926-3373(95)00026-7.

[21] N. Takeda, N. Iwata, T. Torimoto, H. Yoneyama, Influence of carbon black as an adsorbent used in TiO2 photocatalyst films on photodegradation behaviors of propyzamide, J. Catal. 177 (1998) 240–246, http://dx.doi.org/10.1006/jcat.1998.2117.

[22] R. Molinari, M. Mungari, E. Drioli, A. Di Paola, V. Loddo, L. Palmisano, M. Schiavello, Study on a photocatalytic membrane reactor for water purification, Catal. Today. 55 (2000) 71–78, http://dx.doi.org/10.1016/S0920-5861(99)00227-8.

[23] G.E. Romanos, C.P. Athanasekou, F.K. Katsaros, N.K. Kanellopoulos, D.D. Dionysiou, V. Likodimos, P. Falaras, Double-side active TiO2-modified nanofiltration membranes in continuous flow photocatalytic reactors for effective water purification, J. Hazard. Mater. 211–212 (2012) 304–316, http://dx.doi.org/10.1016/j.jhazmat.2011.09.081.

[24] C.P. Athanasekou, G.E. Romanos, F.K. Katsaros, K. Kordatos, V. Likodimos, P. Falaras, Very efficient composite titania membranes in hybrid ultrafiltration/photocatalysis water treatment processes, J. Memb. Sci. 392–393 (2012) 192–203, http://dx.doi.org/10.1016/j.memsci.2011.12.028.

[25] S.K. Papageorgiou, F.K. Katsaros, E.P. Favvas, G.E. Romanos, C.P. Athanasekou, K.G. Beltsios, O.I. Tzialla, P. Falaras, Alginate fibers as photocatalyst immobilizing agents applied in hybrid photocatalytic/ultrafiltration water treatment processes, Water Res. 46 (2012) 1858–1872, http://dx.doi.org/10.1016/j.watres.2012.01.005.

[26] G.E. Romanos, C.P. Athanasekou, V. Likodimos, P. Aloupogiannis, P. Falaras, Hybrid ultrafiltration/photocatalytic membranes for efficient water treatment, Ind. Eng. Chem. Res. 52 (2013) 13938–13947, http://dx.doi.org/10.1021/ie303475b.

[27] N. Ma, X. Quan, Y. Zhang, S. Chen, H. Zhao, Integration of separation and photocatalysis using an inorganic membrane modified with Si-doped TiO2 for water purification, J. Memb. Sci. 335 (2009) 58–67, http://dx.doi.org/10.1016/j.memsci.2009.02.040.

[28] M. Hatat-Fraile, J. Mendret, M. Rivallin, S. Brosillon, Effect of hydrodynamics during sol–gel synthesis of TiO2 nanoparticles: From morphology to photocatalytic properties, Chem. Eng. Res. Des. 91 (2013) 2389–2400, http://dx.doi.org/10.1016/j.cherd.2013.04.022.

[29] S. Adjimi, N. Sergent, J.-C. Roux, F. Delpech, M. Pera-Titus, K. Chhor, A. Kanaev, P.-X. Thivel, Photocatalytic paper based on sol–gel titania nanoparticles immobilized on porous silica for VOC abatement, Appl. Catal. B Environ. 154–155 (2014) 123–133, http://dx.doi.org/10.1016/j.apcatb.2014.02.011.

[30] M.M.H. Fraile, Etude des méthodes d'élaboration et de la mise en oeuvre de photocatalyseurs pour le traitement de la micro pollution bio-réfractaire dans l'eau, Montpellier 2, 2013. http://www.theses.fr/2013MON20043 (accessed March 12, 2015).

[31] C.J. Brinker, G.W. Scherer, Sol-Gel Science: The Physics and Chemistry of Sol-Gel Processing, Elsevier Science, 2013 https://books.google.com/books?hl=en&lr=&id=CND1BAAAQBAJ&pgis=1 (accessed March 12, 2015).

[32] M. Rivallin, M. Benmami, A. Kanaev, A. Gaunand, Sol-gel reactor with rapid micromixing, Chem. Eng. Res. Des. 83 (2005) 67–74, http://dx.doi.org/10.1205/cherd.03073.

[33] S. Mozia, Photocatalytic membrane reactors (PMRs) in water and wastewater treatment. A review, Sep. Purif. Technol. 73 (2010) 71–91, http://dx.doi.org/10.1016/j.seppur.2010.03.021.

[34] M. Pelaez, N.T. Nolan, S.C. Pillai, M.K. Seery, P. Falaras, A.G. Kontos, P.S.M. Dunlop, J.W.J. Hamilton, J.A. Byrne, K. O'Shea, M.H. Entezari, D.D. Dionysiou, A review on the visible light active titanium dioxide photocatalysts for environmental applications, Appl. Catal. B Environ. 125 (2012) 331–349, http://dx.doi.org/10.1016/j.apcatb.2012.05.036.

[35] H. Irie, Y. Watanabe, K. Hashimoto, Nitrogen-concentration dependence on photocatalytic activity of TiO 2 - x N x powders, J. Phys. Chem. B. 107 (2003) 5483–5486, http://dx.doi.org/10.1021/jp030133h.

[36] Y. Park, W. Kim, H. Park, T. Tachikawa, T. Majima, W. Choi, Carbon-doped TiO2 photocatalyst synthesized without using an external carbon precursor and the visible light activity, Appl. Catal. B Environ. 91 (2009) 355–361, http://dx.doi.org/10.1016/j.apcatb.2009.06.001.

[37] N. Sakai, R. Wang, A. Fujishima, T. Watanabe, K. Hashimoto, Effect of ultrasonic treatment on highly hydrophilic TiO 2 surfaces, Langmuir. 14 (1998) 5918–5920, http://dx.doi.org/10.1021/la980623e.

[38] W. Choi, A. Termin, M.R. Hoffmann, The role of metal ion dopants in quantum-sized TiO2: correlation between photoreactivity and charge carrier recombination dynamics, J. Phys. Chem. 98 (1994) 13669–13679, http://dx.doi.org/10.1021/j100102a038.

[39] X. Chen, S.S. Mao, Titanium dioxide nanomaterials: synthesis, properties, modifications, and applications, Chem. Rev. 107 (2007) 2891–2959, http://dx.doi.org/10.1021/cr0500535.

[40] J.-C. Xu, M. Lu, X.-Y. Guo, H.-L. Li, Zinc ions surface-doped titanium dioxide nanotubes and its photocatalysis activity for degradation of methyl orange in water, J.

Mol. Catal. A Chem. 226 (2005) 123–127, http://dx.doi.org/10.1016/j.molcata.2004.09.051.
[41] R. Janes, Structural and spectroscopic studies of iron (III) doped titania powders prepared by sol-gel synthesis and hydrothermal processing, Dye. Pigment. 62 (2004) 199–212, http://dx.doi.org/10.1016/j.dyepig.2003.12.003.
[42] F. Peng, L. Cai, H. Yu, H. Wang, J. Yang, Synthesis and characterization of substitutional and interstitial nitrogen-doped titanium dioxides with visible light photocatalytic activity, J. Solid State Chem. 181 (2008) 130–136, http://dx.doi.org/10.1016/j.jssc.2007.11.012.
[43] Y. Ao, J. Xu, D. Fu, C. Yuan, A simple method to prepare N-doped titania hollow spheres with high photocatalytic activity under visible light, J. Hazard. Mater. 167 (2009) 413–417, http://dx.doi.org/10.1016/j.jhazmat.2008.12.139.
[44] F. Peng, L. Cai, L. Huang, H. Yu, H. Wang, Preparation of nitrogen-doped titanium dioxide with visible-light photocatalytic activity using a facile hydrothermal method, J. Phys. Chem. Solids. 69 (2008) 1657–1664, http://dx.doi.org/10.1016/j.jpcs.2007.12.003.
[45] P. Silija, Z. Yaakob, M.A. Yarmo, S. Sugunan, N.N. Binitha, Visible light active anion codoped sol gel titania photocatalyst for pollutant degradation, J. Sol-Gel Sci. Technol. 59 (2011) 252–259, http://dx.doi.org/10.1007/s10971-011-2491-y.
[46] J. Yu, M. Zhou, B. Cheng, X. Zhao, Preparation, characterization and photocatalytic activity of in situ N, S-codoped TiO2 powders, J. Mol. Catal. A Chem. 246 (2006) 176–184, http://dx.doi.org/10.1016/j.molcata.2005.10.034.
[47] T.C. Jagadale, S.P. Takale, R.S. Sonawane, H.M. Joshi, S.I. Patil, B.B. Kale, S.B. Ogale, N-Doped TiO 2 nanoparticle based visible light photocatalyst by modified peroxide sol − gel method, J. Phys. Chem. C. 112 (2008) 14595–14602, http://dx.doi.org/10.1021/jp803567f.
[48] N. Lu, H. Zhao, J. Li, X. Quan, S. Chen, Characterization of boron-doped TiO2 nanotube arrays prepared by electrochemical method and its visible light activity, Sep. Purif. Technol. 62 (2008) 668–673, http://dx.doi.org/10.1016/j.seppur.2008.03.021.
[49] W. Ho, J.C. Yu, S. Lee, Low-temperature hydrothermal synthesis of S-doped TiO2 with visible light photocatalytic activity, J. Solid State Chem. 179 (2006) 1171–1176, http://dx.doi.org/10.1016/j.jssc.2006.01.009.
[50] A. Fujishima, X. Zhang, D. Tryk, TiO2 photocatalysis and related surface phenomena, Surf. Sci. Rep. 63 (2008) 515–582, http://dx.doi.org/10.1016/j.surfrep.2008.10.001.
[51] M. Hatat-Fraile, J. Mendret, M. Rivallin, S. Brosillon, Photocatalytic membranes for the treatment of refractory organic pollutants, Procedia Eng. 44 (2012) 440–442, http://dx.doi.org/10.1016/j.proeng.2012.08.442.
[52] A.N. Kadam, R.S. Dhabbe, M.R. Kokate, Y.B. Gaikwad, K.M. Garadkar, Preparation of N doped TiO2 via microwave-assisted method and its photocatalytic activity for degradation of Malathion, Spectrochim Acta Part A Mol. Biomol. Spectrosc. 133 (2014) 669–676, http://dx.doi.org/10.1016/j.saa.2014.06.020.
[53] J. Tauc, R. Grigorovici, A. Vancu, Optical properties and electronic structure of amorphous germanium, Phys. Status Solidi. 15 (1966) 627–637, http://dx.doi.org/10.1002/pssb.19660150224.
[54] H. Lin, C. Huang, W. Li, C. Ni, S. Shah, Y. Tseng, Size dependency of nanocrystalline TiO2 on its optical property and photocatalytic reactivity exemplified by 2-chlorophenol, Appl. Catal. B Environ. 68 (2006) 1–11, http://dx.doi.org/10.1016/j.apcatb.2006.07.018.
[55] A. Galenda, L. Crociani, N. El Habra, M. Favaro, M.M. Natile, G. Rossetto, Effect of reaction conditions on methyl red degradation mediated by boron and nitrogen doped TiO2, Appl. Surf. Sci. 314 (2014) 919–930, http://dx.doi.org/10.1016/j.apsusc.2014.06.175.
[56] Y. Cong, J. Zhang, F. Chen, M. Anpo, Synthesis and characterization of nitrogen-doped TiO2 nanophotocatalyst with high visible light activity, J. Phys. Chem. C. 111 (2007) 6976–6982, http://dx.doi.org/10.1021/jp0685030.
[57] R.R. Bhosale, S.R. Pujari, G.G. Muley, S.H. Patil, K.R. Patil, M.F. Shaikh, A.B. Gambhire, Solar photocatalytic degradation of methylene blue using doped TiO2 nanoparticles, Sol. Energy. 103 (2014) 473–479, http://dx.doi.org/10.1016/j.solener.2014.02.043.
[58] L. Li, Y. Yang, X. Liu, R. Fan, Y. Shi, S. Li, L. Zhang, X. Fan, P. Tang, R. Xu, W. Zhang, Y. Wang, L. Ma, A direct synthesis of B-doped TiO2 and its photocatalytic performance on degradation of RhB, Appl. Surf. Sci. 265 (2013) 36–40, http://dx.doi.org/10.1016/j.apsusc.2012.10.075.
[59] D.H. Quiñones, A. Rey, P.M. Álvarez, F.J. Beltrán, G. Li Puma, Boron doped TiO2 catalysts for photocatalytic ozonation of aqueous mixtures of common pesticides: Diuron, o-phenylphenol, MCPA and terbuthylazine, Appl. Catal. B Environ. 178 (2015) 74–81, http://dx.doi.org/10.1016/j.apcatb.2014.10.036.
[60] Y. Huang, W. Ho, Z. Ai, X. Song, L. Zhang, S. Lee, Aerosol-assisted flow synthesis of B-doped, Ni-doped and B-Ni-codoped TiO2 solid and hollow microspheres for photocatalytic removal of NO, Appl. Catal. B Environ. 89 (2009) 398–405, http://dx.doi.org/10.1016/j.apcatb.2008.12.020.
[61] W. Göpel, J. Anderson, D. Frankel, M. Jaehnig, K. Phillips, J. Schäfer, G. Rocker, Surface defects of TiO2(110): A combined XPS, XAES AND ELS study, Surf. Sci. 139 (1984) 333–346, http://dx.doi.org/10.1016/0039-6028(84)90054-2.
[62] Z. Xiong, X.S. Zhao, Nitrogen-doped titanate-anatase core-shell nanobelts with exposed 101 anatase facets and enhanced visible light photocatalytic activity, J. Am. Chem. Soc. 134 (2012) 5754–5757, http://dx.doi.org/10.1021/ja300730c.
[63] R.P. Cavalcante, R.F. Dantas, B. Bayarri, O. González, J. Giménez, S. Esplugas, A. Machulek, Synthesis and characterization of B-doped TiO2 and their performance for the degradation of metoprolol, Catal. Today. 252 (2015) 27–34, http://dx.doi.org/10.1016/j.cattod.2014.09.030.
[64] H. Strathmann, Introduction to Membrane Science and Technology, Wiley, 2011, http://www.wiley-vch.de/publish/en/AreaOfInterestCG00/availableTitles/3-527-32451-8/?sID=b72uu95nh8skhcmra24ef1cde1 (accessed February 22, 2016).
[65] R. Wang, K. Hashimoto, A. Fujishima, M. Chikuni, E. Kojima, A. Kitamura, M. Shimohigoshi, T. Watanabe, Photogeneration of highly amphiphilic TiO2 surfaces, Adv. Mater. 10 (1998) 135–138, http://dx.doi.org/10.1002/(SICI)1521-4095(199801)10:2<135::AID-ADMA135>3.0.CO;2-M.
[66] N. Stevens, C.I. Priest, R. Sedev, J. Ralston, Wettability of photoresponsive titanium dioxide surfaces, Langmuir 19 (8) (2003) 3272–3275, http://dx.doi.org/10.1021/LA020660C.
[67] M. Miyauchi, A. Nakajima, A. Fujishima, K. Hashimoto, T. Watanabe, Photoinduced surface reactions on TiO_2 and $SrTiO_3$ films: photocatalytic oxidation and photoinduced hydrophilicity, Chem. Mater. 12 (1) (2000) 3–5, http://dx.doi.org/10.1021/CM990556P.
[68] R. Wang, K. Hashimoto, A. Fujishima, M. Chikuni, E. Kojima, A. Kitamura, M. Shimohigoshi, T. Watanabe, Light-induced amphiphilic surfaces 388 (1997) 431–432, http://dx.doi.org/10.1038/41233.
[69] V. Gekas, B. Hallström, Microfiltration membranes, cross-flow transport mechanisms and fouling studies, Desalination. 77 (1990) 195–218, http://dx.doi.org/10.1016/0011-9164(90)85026-7.
[70] P. Ramesh Babu, V.G. Gaikar, Membrane characteristics as determinant in fouling of UF membranes, Sep. Purif. Technol. 24 (2001) 23–34, http://dx.doi.org/10.1016/S1383-5866(00)00207-0.
[71] H.Y. Lee, Y.H. Park, K.H. Ko, Correlation between surface morphology and hydrophilic/hydrophobic conversion of MOCVD − TiO 2 Films, Langmuir 16 (2000) 7289–7293, http://dx.doi.org/10.1021/la9915567.
[72] N.P. Xekoukoulotakis, D. Mantzavinos, R. Dillert, D. Bahnemann, Synthesis and photocatalytic activity of boron-doped TiO(2) in aqueous suspensions under UV-A irradiation, Water Sci. Technol. 61 (2010) 2501–2506, http://dx.doi.org/10.2166/wst.2010.150.
[73] A. Zaleska, J.W. Sobczak, E. Grabowska, J. Hupka, Preparation and photocatalytic activity of boron-modified TiO2 under UV and visible light, Appl. Catal. B Environ. 78 (2008) 92–100, http://dx.doi.org/10.1016/j.apcatb.2007.09.005.
[74] R. Asahi, Visible-Light Photocatalysis in Nitrogen-Doped Titanium Oxides, Science 293 (2001) 269–271, http://dx.doi.org/10.1126/science.1061051.
[75] J. Mendret, M. Hatat-Fraile, M. Rivallin, S. Brosillon, Hydrophilic composite membranes for simultaneous separation and photocatalytic degradation of organic pollutants, Sep. Purif. Technol. 111 (2013) 9–19, http://dx.doi.org/10.1016/j.seppur.2013.03.030.